Chemistry
A European
Journal

Chemistry
Europe
European Chemical
Societies Publishing

Reprint

WILEY-VCH

Photodynamic Therapy |Hot Paper|

Photocytotoxicity of Oligothienyl-Functionalized Chelates That Sensitize Ln^{III} Luminescence and Generate $^1O_2$

Katherine R. Johnson,[a] Vincent C. Lombardi,[b] and Ana de Bettencourt-Dias*[a]

Abstract: Three new compounds containing a heptadentate lanthanide (Ln^{III}) ion chelator functionalized with oligothiophenes, ***n*Thept(COOH)$_4$** ($n=1$, 2, or 3), were isolated. Their Ln^{III} complexes not only display the characteristic metal-centered emission in the visible or near-infrared (NIR) but also generate singlet oxygen ($^1O_2$). Luminescence efficiencies (φ^{Ln}) for [Eu***1*Thept(COO)$_4$**]$^-$ and [Eu***2*Thept(COO)$_4$**]$^-$ are $\varphi^{Eu}=3\%$ and 0.5% in TRIS buffer and 33% and 3% in 95% ethanol, respectively. ***3*Thept(COO)$_4^{4-}$** does not sensitize Eu^{III} emission due to its low-lying triplet state. Near infra-red (NIR) luminescence is observed for all NIR-emitting Ln^{III} and ligands with efficiencies of $\varphi^{Yb}=0.002\%$, 0.005% and 0.04% for [Yb***n*Thept(COO)$_4$**]$^-$ ($n=1$, 2, or 3), and $\varphi^{Nd}=0.0007\%$, 0.002% and 0.02% for [Nd***n*Thept(COO)$_4$**]$^-$ ($n=1$, 2, or 3) in TRIS buffer. In 95% ethanol, quantum yields of NIR luminescence increase and are $\varphi^{Yb}=0.5\%$, 0.31% and 0.05% for [Yb***n*Thept(COO)$_4$**]$^-$ ($n=1$, 2, or 3), and $\varphi^{Nd}=0.40\%$, 0.45% and 0.12% for [Nd***n*Thept(COO)$_4$**]$^-$ ($n=1$, 2, or 3). All complexes are capable of generating $^1O_2$ in 95% ethanol with φ_{1O2} efficiencies which range from 2% to 29%. These complexes are toxic to HeLa cells when irradiated with UV light ($\lambda_{exc}=365$ nm) for two minutes. IC_{50} values for the Ln^{III} complexes are in the range 15.2–16.2 μM; the most potent compound is [Nd***2*Thept(COO)$_4$**]$^-$. The cell death mechanisms are further explored using an Annexin V—propidium iodide assay which suggests that cell death occurs through both apoptosis and necrosis.

Introduction

Singlet oxygen ($^1O_2$) is a reactive oxygen species directly linked to cellular death and tissue damage.[1] Photosensitizers that efficiently generate $^1O_2$ are useful in photodynamic therapy (PDT).[2] [3] Porfimer sodium, or Photofrin, was approved by the U.S. Food and Drug Administration in 1993 for the treatment of bladder cancer and has since been approved for several other cancers, including endobronchial and esophageal cancers.[4] Most compounds studied for PDT applications are porphyrin-based. However, they suffer from many drawbacks, including aggregation, which shortens the lifetime of the excited state resulting in lower $^1O_2$ generation quantum yields,[5] and poor solubility.[6] These drawbacks limit dosage concentration and performance.[7] To circumvent these issues, there is a fundamental interest in the development of new types of $^1O_2$ generators that are just as effective.[8] Ideal photosensitizers for PDT need to be chemically pure, photostable, and effective at low doses for advanced cancer therapy. Compounds with additional properties, such as luminescence for *in situ* or *in vivo* imaging, have an additional advantage.[9]

Lanthanide ion (Ln^{III}) luminescence is highly desirable for imaging purposes due to characteristic emission wavelengths, large pseudo-Stokes shifts of sensitized emission, and long decay lifetimes. The latter enable time-gated detection of the emission resulting in improved signal-to-noise ratios.[10] The metal-centered emission is based on transitions within the 4*f* orbitals. These intraconfigurational transitions are parity-forbidden, which poses a challenge for direct excitation. To overcome this, coordinated ligands are used to transfer energy to the Ln^{III}. This sensitization process is referred to as the antenna effect (Figure 1).[10]

Ln^{III}-based systems work well as multifunctional platforms with imaging capabilities.[11, 12, 13] Patra and coworkers described Eu^{III} and Tb^{III} complexes with dipyrido[3,2-d:2′,3′-f]quinoxaline (dbq) and 4,4,4-trifluoro-1-(2-napthyl)-1,3-butanedione (tfnb) sensitizers. These complexes penetrate the cell membrane of H460 and MCF-7 cells. The IC_{50} value of the most phototoxic complex, [Tb(dpq)(tfnb)$_3$], was reported as 7.94 ± 0.65 μM (H460 cells).[14] Although the authors mention that the cells remained viable in the presence of the complexes under dark conditions, IC_{50} values for dark toxicity were not reported. A Tb^{III} DOTA-based complex that displays a green Tb^{III}-centered emission with an emission efficiency (φ^{Tb}) of 24% and $^1O_2$ generation efficiency ($\varphi_{^1O_2}$) of 12% was used to image NIH-3T3 cells.[15] While φ^{Tb} is high, $\varphi_{^1O_2}$ falls well below the efficiencies of naturally occurring organic photosensitizers.[8] Ung, Gasser, and coworkers described Tb^{III} complexes and their photocyto-

[a] Dr. K. R. Johnson, Prof. Dr. A. de Bettencourt-Dias
Department of Chemistry, University of Nevada, Reno
Reno, NV 89557 (USA)
E-mail: abd@unr.edu

[b] Prof. Dr. V. C. Lombardi
Department of Microbiology and Immunology
University of Nevada, Reno, Reno, NV 89557 (USA)

Supporting information and the ORCID identification number(s) for the author(s) of this article can be found under:
https://doi.org/10.1002/chem.202001568.

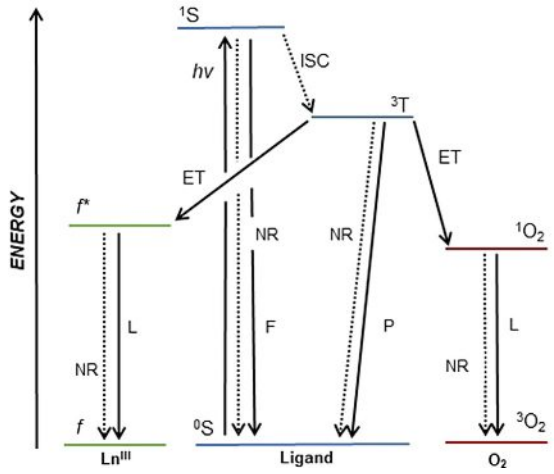

Figure 1. Energy level diagram showing the energy transfer (ET) pathways for both Ln^{III} sensitization and $^1O_2$ generation. Energy $h\nu$ is absorbed by the ligand to populate a singlet excited state (^{1}S). Intersystem crossing (ISC) leads to population of a triplet excited state (^{3}T). This state can then transfer energy to populate the emissive f* excited state which decays by luminescence (L) to the ground state, f. Alternatively, the energy transfer leads to $^1O_2$ generation, which decays to triplet oxygen $^3O_2$ by emitting at 1270 nm. Nonradiative (NR), dash-dot lines) pathways lead to quenching of excited states. Competing radiative processes are fluorescence (F) and phosphorescence (P). Energy levels are not drawn to scale.

toxicity against HeLa and MRC-5 cells. After treatment, the cell morphology of HeLa cells changed, which, coupled with cell viability studies, indicates compound toxicity. IC_{50} values were reported between 14.3 and 32.3 μM (HeLa cells).[16] An Er^{III} porphyrin-based complex that displays Er^{III}-centered emission in the near-infrared and $^1O_2$ generation was used to image HeLa cells and shown to localize in the cell mitochondria.[17] Although this complex displayed photocytotoxicity, the reported $\varphi_{^1O_2}$ of 10% is much lower than reported efficiencies of other photosensitizers.[8]

Our group has recently described naphthalimide-based complexes that sensitize visible (Eu^{III}) and near-infrared (Yb^{III}, Nd^{III}) emitting ions in addition to generating $^1O_2$ with $\varphi_{^1O_2}$ in the range 41–64%.[18] However, these compounds are not water-soluble, and thus, not useful for imaging and therapy in biological systems. 2,2′-Bithiophene and 2,2′:5′,2″-terthiophene are biologically active natural products present in a variety of plants. Their toxicity and ability to generate $^1O_2$ with high $\varphi_{^1O_2}$ have been well documented.[19] Oligothiophene-based systems have shown promise in photodynamic therapy for the treatment of bladder carcinomas[20] and fibrosarcoma cells.[21] Our group recently described terthiophene-based, luminescent Ln^{III} complexes with wavelength-dependent $^1O_2$ generation.[22] Thus, we aimed to isolate Ln^{III} complexes based on three different oligothiophenes that display luminescence and generate $^1O_2$ in aqueous systems.

As Ln^{III} can be toxic to living systems,[23] chelators with high complex stability are used and we selected 2,2′,2″,2‴-[(2,6-pyridinediylbis(methylenenitrilo)]tetraacetic acid. This compound is known for its stability in aqueous solution with a pGd value, which is -log[concentration] of free Gd^{III} in solution in the presence of the chelator, of 17.5 and is comparable to other metal chelators such as diethylenetriamine pentaacetate under the same conditions (pGd = 19.1).[24] We report the isolation of oligothienyl-derivatized of 2,2′,2″,2‴-[(2,6-pyridinediylbis(methylenenitrilo)]tetraacetic acid-based photosensitizers, ***n*Thept-(COOH)$_4$** (Scheme 1), and the luminescence and cytotoxic properties of their Ln^{III} complexes (Ln^{III} = Eu^{III}, Yb^{III}, or Nd^{III}), along with the mechanism of cell death. These complexes are water-soluble and show Ln^{III}-centered emission in either the visible (Eu^{III}) or near infrared (NIR) range (Yb^{III} or Nd^{III}) while generating $^1O_2$.

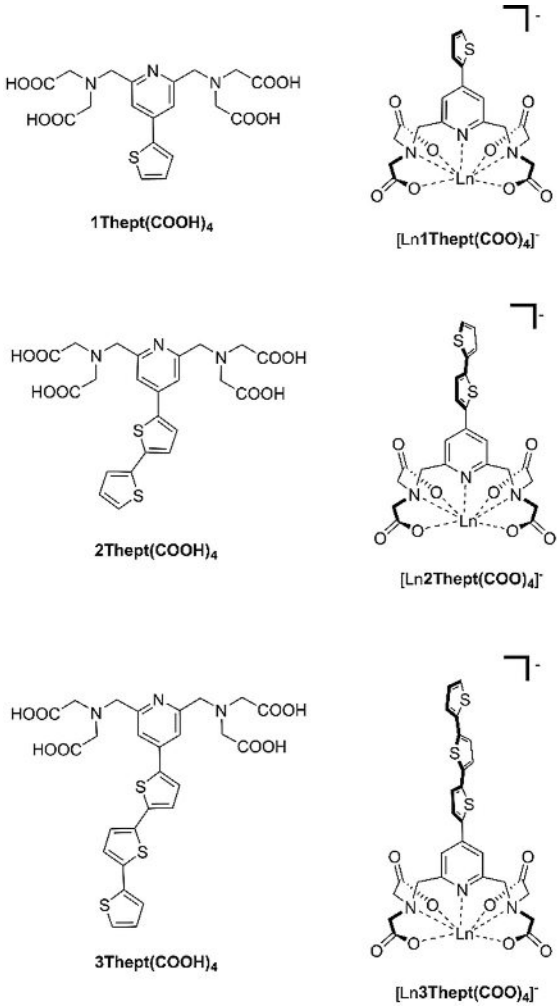

Scheme 1. The compounds ***n*Thept(COOH)$_4$** and [Ln***n*Thept(COO)$_4$]$^-$ (n = 1, 2, or 3) studied here. The coordination sphere of the Ln^{III} ions is completed by molecules that are not shown (see text).

Results and Discussion

***n*Thept(COOH)$_4$** (n = 1, 2, or 3; Scheme 1) were synthesized through a Pd-catalyzed Suzuki–Miyaura cross-coupling between 4-bromo-2,6-bis[*N*,*N*-bis(ethoxycarbonylmethyl)aminomethyl]pyridine and the respective borolanes to yield the diethyl ester derivatives in 33–56% yield (Figure S1, Supporting Information). The esters were saponified to yield the water-

Table 1. Quantum yields of fluorescence (φ^F) and of Ln^{III} luminescence (φ^{Ln}) for ***n*Thept(COO)$_4^{4-}$** ($n=1$, 2, or 3) and their Ln^{III} complexes, and luminescence lifetime (τ^{Eu}), intrinsic quantum yield (φ^{Eu}_{Eu}), and sensitization efficiency (η_{sens}), for [Eu**1Thept(COO)$_4$**]$^-$ measured at 25.0±0.1 °C.

	Solvent	φ^F no Ln^{III} [%]	φ^F $Ln^{III}=Gd^{III}$ [%]	φ^{Yb} [%]	τ^{Yb} [ms]	φ^{Nd} [%]	φ^{Eu} [%]	τ^{Eu} [ms]	φ^{Eu}_{Eu} [%]	η_{sens} [%]	q (Eu^{III})
[Ln**1Thept(COO)$_4$**]$^-$	TRIS buffer	5.3±0.2	32±2	0.002±0.000	[a]	0.0007 ±.0000	3.1±0.0	0.39±0.01	10	31	1.9 ±0.1
	95% EtOH	19±0	19±0	0.50±0.01	4.03±0.04	0.40±0.04	32.6±0.2	1.3±0.00	10	82	
[Ln**2Thept(COO)$_4$**]$^-$	TRIS buffer	6.3±0.8	20±0	0.005±0.000	[a]	0.002 ±0.000	0.53±0.01	[a]	[a]	[a]	
	95% EtOH	18±1	13±0	0.31±0.01	4.19±0.00	0.45 ±0.05	3.0±0.0	0.39±0.01	10.3	29	
[Ln**3Thept(COO)$_4$**]$^-$	TRIS buffer[b]	4.7±0.2	27±1	0.04±0.00	[a]	0.02 ±.00	[c]	[c]	[c]	[c]	
	95% EtOH	13±0	19±0	0.05±0.00	3.99±0.00	0.12 ±0.00	[c]	[c]	[c]	[c]	

[a] Luminescence was too weak. [b] In TRIS buffer with 15% DMSO. [c] Eu^{III} luminescence was not observed.

soluble compounds, ***n*Thept(COOH)$_4$** ($n=1$, 2, or 3), in 90–94% yield. Their isolation was confirmed by NMR spectroscopy and mass spectrometry (Figures S2–S10).

Ln^{III} complexes were prepared by deprotonating the ligands with K_2CO_3 and mixing in a 1:1 stoichiometry with the $LnCl_3$ salt ($Ln^{III}=Gd^{III}$, Eu^{III}, Yb^{III}, or Nd^{III}) in 1:1 water: methanol and heated to 60 °C. After solvent evaporation, the complexes were recovered as white, yellow, and brown salts for K[Ln**1Thept(COO)$_4$**], K[Ln**2Thept(COO)$_4$**], and K[Ln**3Thept(COO)$_4$**], respectively, in 89–96% yield. The complexes were characterized using mass spectrometry (Figures S14–S24). For spectroscopy, the Ln^{III} complexes were prepared in solution and not isolated.

Speciation studies of **1Thept(COO)$_4^{4-}$**, **2Thept(COO)$_4^{4-}$**, and **3Thept(COO)$_4^{4-}$** with $LnCl_3$ ($Ln^{III}=Yb^{III}$ or Eu^{III}) (Figures S11–S13) confirm the formation of 1:1 complexes, as expected.[24,25]

All deprotonated ligands (***n*Thept(COO)$_4^{4-}$**) display absorptions with maxima at 300 nm, 360 nm, and 400 nm for $n=1$, 2 or 3 in TRIS buffer. Exciting ***n*Thept(COO)$_4^{4-}$** ($n=1$, 2, or 3) at these absorbance maxima results in structureless fluorescence bands in the UV-visible region with maxima at 365, 460, and 525 nm, respectively (Figures S25–S27). The bathochromic shifts observed in the absorbance and emission spectra from $n=1$ to 3 are consistent with increased π-conjugation and decreased HOMO–LUMO gap.[26] The profiles of the absorption, excitation, and emission spectra of the Gd^{III} complexes, [Gd***n*Thept(COO)$_4$**]$^-$, exhibit analogous behavior to the free ligands in TRIS buffer (Figures S28–S30), but with a significant increase in emission intensity (Figures S31–S33). This is consistent with planarization of the ligand upon coordination[27] and some phosphorescence contribution due to improved ISC. Fluorescence quantum yields (φ^F) were determined from the emission spectra (Figures S31-S33) for the free ligands and Gd^{III} complexes. ***n*Thept(COO)$_4^{4-}$** efficiencies are 5.3% for $n=1$, 6.3% for $n=2$, and 4.7% for $n=3$. φ^F of [Gd***n*Thept(COO)$_4$**]$^-$ are 32% for $n=1$, 20% for $n=2$, and 27% for $n=3$ (Table 1).

The [Ln***n*Thept(COO)$_4$**]$^-$ complexes emit in the visible ($Ln^{III}=Eu^{III}$) and NIR ($Ln^{III}=Nd^{III}$ or Yb^{III}) in TRIS buffer. The emission spectra of [Eu***1*Thept(COO)$_4$**]$^-$, [Yb***1*Thept(COO)$_4$**]$^-$, and [Nd***1*Thept(COO)$_4$**]$^-$, shown in Figure 2, display the characteristic metal-centered narrow transitions. For [Eu***1*Thept(COO)$_4$**]$^-$, the presence of the $^5D_0\rightarrow{}^7F_0$ band is consistent with a low symmetry environment around the metal ion.[28] ***2*Thept(COO)$_4^{4-}$** also sensitizes Eu^{III}, but with poor efficiency, as evidenced by residual ligand emission (Figure S43). A similar behavior is observed in ethanol, and, in this solvent, we were able to determine the sensitization efficiency η_{sens} (Table 1), which is low at 29% (*vide infra*). This is consistent with a ^3T state that is very close in energy to the emissive state of Eu^{III}.[18] Quantum yields of Eu^{III} emission (φ^{Eu}) were 3.1% and 0.53% for [Eu***1*Thept(COO)$_4$**]$^-$ and [Eu***2*Thept(COO)$_4$**]$^-$, respectively (Table 1). The luminescence lifetime (τ^{Eu}) of [Eu***1*Thept(COO)$_4$**]$^-$ is 0.39 ms and was fit as a single-exponential decay (Figure S46), consistent with a unique coordination environment around the Eu^{III} ion.[10,29] We were unable to measure the emission lifetime of the [*Eu**2Thept**(COO)$_4$*]$^-$ complex due to the weak emission.

Complexes containing NIR emitting Ln^{III} ions, [Yb***n*Thept(COO)$_4$**]$^-$ and [Nd***n*Thept(COO)$_4$**]$^-$, display the characteristic Ln^{III} emission bands (Figures 2 and S43, S44). Quantum yields of Yb^{III} and Nd^{III} emission (φ^{Yb} and φ^{Nd}) are summarized in Table 1. [Yb***1*Thept(COO)$_4$**]$^-$ and [Nd***1*Thept(COO)$_4$**]$^-$ display

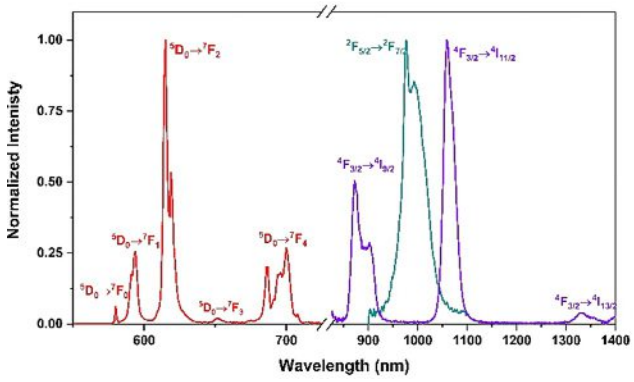

Figure 2. Normalized emission spectra of [Ln(**1Thept(COO)$_4$**)]$^-$ ($Ln^{III}=Eu^{III}$ (red), Yb^{III} (teal), or Nd^{III} (purple)) in TRIS buffer. ($\lambda_{exc}=310$ nm; [compound] $=1\times10^{-4}$ M).

the lowest quantum efficiencies of the series at 0.002% and 0.0007%, respectively. The efficiencies for [Yb***2*Thept(COO)$_4$]$^-$ and [Nd***2*Thept(COO)$_4$]$^-$ are 0.005% and 0.002%, respectively. The largest efficiencies are observed for [Yb***3*Thept(COO)$_4$]$^-$ and [Nd***3*Thept(COO)$_4$]$^-$ and are 0.04% and 0.02%, respectively. These results are similar to what has been observed for other Ln^{III} species.[25b,c]

As the deprotonated ligand is heptadentate, we expect the coordination sphere of the Ln^{III} ions to be completed by coordinated water molecules. Comparison of the emission lifetimes for Eu^{III} in H_2O and D_2O (Figures S47 and S48),[30] indicated that the number of coordinated water molecules q for [Eu(***1*Thept-(COO)$_4$]$^-$ is ≈2 (Table S1). This corresponds to a coordination number of 9, and is consistent to what is reported for this chelator in other Ln^{III} ion complexes.[24,25c,31] Due to the similar sizes of the Ln^{III} ions, we expect a similar coordination number for all complexes.

In 95% ethanol, the absorption, emission, and excitation spectra of ***n*Thept(COO)$_4^{4-}$** and [Gd***n*Thept(COO)$_4$]$^-$ display similar profiles to the spectra collected in TRIS buffer (Figures S34–S39). A significant increase in fluorescence emission intensity is observed for each Gd^{III} metal complex compared to the respective free ligand, as was observed in TRIS buffer (Figures S40–S42).

The emission spectra of [Eu***1*Thept(COO)$_4$]$^-$, [Yb***1*Thept-(COO)$_4$]$^-$, and [Nd***1*Thept(COO)$_4$]$^-$ in 95% ethanol (Figure S49a) are analogous to the ones in TRIS buffer. ***2*Thept-(COO)$_4^{4-}$** also sensitizes Eu^{III}, but with poor efficiency, as evidenced by residual ligand emission (Figure S49b). Quantum yields of Eu^{III} emission in 95% ethanol (φ^{Eu}) significantly increase from 3.1% and 0.53% (TRIS buffer) to 33% and 3% for [Eu***1*Thept(COO)$_4$]$^-$ and [Eu***2*Thept(COO)$_4$]$^-$, respectively (Table 1). τ^{Eu} of [Eu***1*Thept(COO)$_4$]$^-$ and [Eu***2*Thept(COO)$_4$]$^-$ are 1.3 and 0.39 ms, respectively (Figures S53 and S55, Table S2). These lifetimes are longer than those measured in TRIS buffer, consistent with the reduced quenching effect by O–H oscillators in 95% ethanol compared to water (Figure S58).[10] The lifetimes enabled us to calculate the η_{sens} for these two complexes as 82 and 29%, respectively, consistent with the observed residual ligand emission mentioned above in the latter case.

For the same reason, φ^{Ln} for the NIR emitting complexes, [Yb***n*Thept(COO)$_4$]$^-$ and [Nd***n*Thept(COO)$_4$]$^-$, were higher in 95% ethanol as well (Table 1). The increase in luminescence intensity enabled measuring the emission lifetimes (τ^{Yb}) of [Yb***n*-Thept(COO)$_4$]$^-$, which were 4.03 μs, 4.19 μs, and 3.99 μs for n=1, 2, and 3, respectively (Figures S54, S56, and S57, Table S2). They are comparable to other Yb^{III} complexes.[32]

$^1O_2$ phosphorescence at 1270 nm, used to determine efficiency of $^1O_2$ generation,[18,22a] was low in TRIS buffer (Figure S45), most likely due the low dissolved O_2 content (water; $\chi_{O_2}=0.2\times10^{-4}$).[33] In ethanol, which has a higher dissolved oxygen content ($\chi_{O_2}=5.71\times10^{-4}$),[34] the phosphorescence is more intense (Figures 3, S51 and S52) and allowed determination of φ_{1O2}. These values are summarized in Table 2 and are 15% for n=1, 12% when n=2, and 24% when n=3, and are comparable to values reported for other thienyl-based compounds.[22a] The Gd^{III} complexes have the largest φ_{1O2} at 27% for [Gd***1*Thept(COO)$_4$]$^-$, 17% for [Gd***2*Thept(COO)$_4$]$^-$, and 29% for [Gd***3*Thept(COO)$_4$]$^-$. This observed increase in $\varphi_{^1O_2}$ from the organic photosensitizers to their Gd^{III} complexes was observed by Maury and coworkers[35] and us[18,22a] as well, and is attributed to the heavy atom effect.[36] $\varphi_{^1O_2}$ was determined to be 16% for [Eu***2*Thept(COO)$_4$]$^-$, 6% for [Yb***2*Thept(COO)$_4$]$^-$, and 2% for [Yb***3*Thept(COO)$_4$]$^-$. Low $^1O_2$ emission intensity is observed for [Ln***1*Thept(COO)$_4$]$^-$ (Ln^{III}=Eu^{III}, Yb^{III}, or Nd^{III}), which prevented us from determining $\varphi_{^1O_2}$. $^1O_2$ phosphorescence is also observed for the Nd^{III} complexes with **2Thept-(COO)$_4^-$** and **3Thept(COO)$_4^-$**; however, due to the intensity of the nearby $^4F_{3/2}\rightarrow{}^4I_{13/2}$ transition, $\varphi_{^1O_2}$ could not be quantified.

We studied the cytotoxicity of ***n*Thept(COO)$_4^{4-}$** (n=1 or 2) and their Ln^{III} complexes towards HeLa cells (Figures 4 and Figure S61). **3Thept(COO)$_4^{4-}$** and its complexes were poorly soluble in TRIS buffer and required 15% DMSO to completely dissolve, thus their cytotoxicity was not studied.[37]

HeLa cells are ideal candidates for PDT studies due to their robust characteristics.[38] The phototoxicity and dark toxicity of our compounds were determined using an MTT metabolic activity assay.[39] As seen in Figure 4, treatment of HeLa cells with solutions of [Ln**2Thept(COO)$_4$]$^-$ or **2Thept(COO)$_4^{4-}$** in 3.13 μM, 6.25 μM, 12.5 μM, or 25 μM concentration in the dark does not appreciably change cell viability. However, at 50 μM and

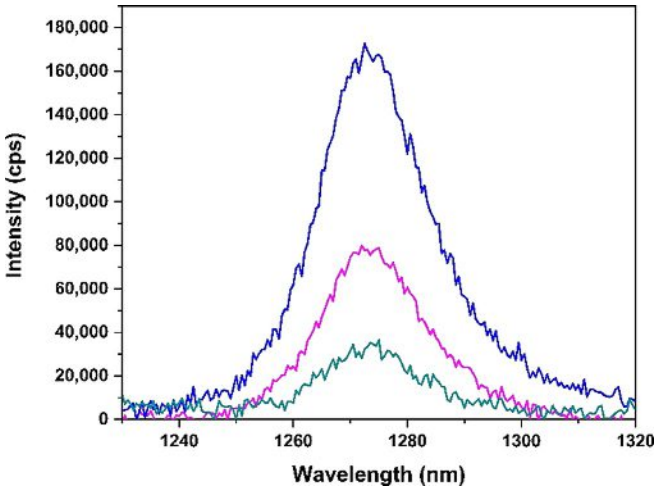

Figure 3. Phosphorescence spectra of $^1O_2$ for solutions in 95% ethanol of **3Thept(COO)$_4^{4-}$** (pink) and [Ln**3Thept(COO)$_4$]$^-$ (Ln^{III}=Gd^{III} (blue), Yb^{III}(teal)). (λ_{exc}=400 nm; [compound]=5×10^{-5} M).

Table 2. Quantum yields of $^1O_2$ generation (φ_{1O2}) for ***n*Thept(COO)$_4^{4-}$** and [Ln***n*Thept(COO)$_4$]$^-$ at 25.0±0.1 °C in 95% ethanol.

	no Ln^{III}	Gd^{III}	Eu^{III}	Yb^{III}	Nd^{III}
[Ln***1*Thept(COO)$_4$]$^-$	15±0	27±1	[a]	[a]	[a]
[Ln***2*Thept(COO)$_4$]$^-$	12±0	17±1	16±1	6±0	[a]
[Ln***3*Thept(COO)$_4$]$^-$	24±0	29±1	[b]	2±0	[a]

[a] Luminescence emission was observed but was too low to quantify. [b] Not studied.

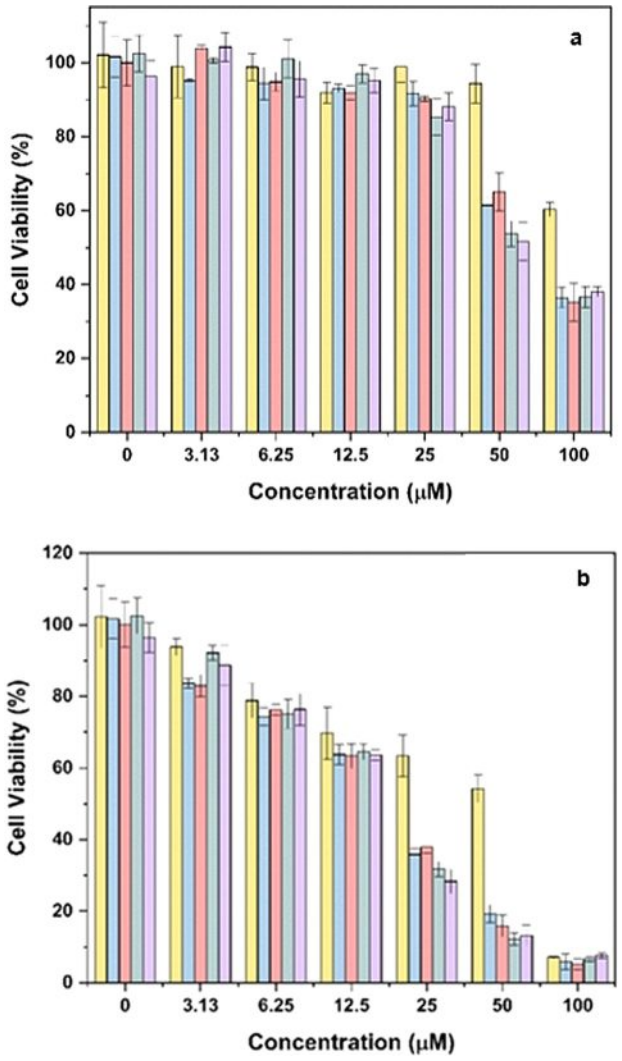

Figure 4. (a) Cell viability (%, MTT assay) as a function of concentration of **2Thept(COO)$_4^{4-}$** (yellow) or [Ln**2Thept(COO)$_4$**]$^-$, in the dark; (b) cell viability (%, MTT assay) as a function of concentration of **2Thept(COO)$_4^{4-}$** or [Ln**2Thept(COO)$_4$**]$^-$, after irradiating for 2 minutes with 365 nm light. The control experiments were performed under the same experimental conditions and correspond to the entries at 0 μM. [Ln^{III} = Gd^{III} (blue), Eu^{III} (salmon) Yb^{III} (green) or Nd^{III} (purple)].

100 μM, cell viabilities decrease below 90%, indicating some dark cytotoxicity at these higher concentrations.

In contrast, the viability of the cells irradiated at 365 nm for 2 minutes decreases with increasing concentration of compound. Cell viability also decreases with increasing irradiation time (Figure S62). As irradiating the cells without added compounds does not lead to a decrease in cell viability, these results suggest that, at concentrations between 3.13 μM and 25 μM, our compounds are photocytotoxic. At the highest concentration tested, cell viabilities range from 8 to 15%.

A dose response fitting was applied to the above data for each compound when irradiated (Figures S63–S72, Tables S3 and S4), and the resulting IC_{50} values are presented in Table 3. These values indicate that the metal complexes are more photocytotoxic than the free ligand, ***2*Thept(COO)$_4^{4-}$**. Also, these compounds are less cytotoxic in the dark than the well-known

Table 3. IC_{50} values of **2Thept(COO)$_4^{4-}$** and [Ln**2Thept(COO)$_4$**]$^-$, in which Ln^{III} = Gd^{III}, Eu^{III}, Yb^{III}, or Nd^{III}, in HeLa cells compared to Photofrin.

	IC_{50} [μM] *hv*	IC_{50} [μM] no *hv*
2Thep(COO)$_4^{4-}$	33.9 ± 4.6	113.4 ± 7.1
[Gd**2Thept(COO)$_4$**]$^-$	16.1 ± 0.7	70.2 ± 3.7
[Eu**2Thept(COO)$_4$**]$^-$	16.2 ± 0.8	71.7 ± 3.5
[Yb**2Thept(COO)$_4$**]$^-$	15.8 ± 0.6	65.4 ± 4.2
[Nd**2Thept(COO)$_4$**]$^-$	15.2 ± 0.7	64.7 ± 4.3
Photofrin[40]	7.1	> 41

photodynamic agent, Photofrin, in HeLa cells.[40] Cell viability of ***1*Thept(COO)$_4^{4-}$** and all [Ln***1*Thept(COO)$_4$**]$^-$ was also studied and shows that these compounds are photocytotoxic (Figure S61), although were not able to fit the data to meaningful IC_{50} values. The photocytotoxicity was not unexpected, as these compounds are capable of generating $^1O_2$ as well.

We investigated the nature of the cell death mechanism for the ***2*Thept(COO)$_4$** series using flow cytometry on Annexin V-FITC/PI-labelled HeLa cells in the dark and when exposed to 365 nm light (Figure 5). The cell population of viable cells (FITC$^-$/PI$^-$), early stage apoptotic cells (FITC$^+$/PI$^-$), late stage apoptotic cells (FITC$^+$/PI$^+$), and necrotic cells (FITC$^-$/PI$^+$) was measured to indicate phases of cell death. In the control groups (a- in the dark, b- light irradiation), less than 10.0% of combined cell death phases were observed at all conditions. Incubating the cells with **2Thept(COO)$_4^{4-}$** in the dark yields results similar to the control experiments. HeLa cells treated with [Ln**2Thept(COO)$_4$**]$^-$ (Ln^{III} = Gd^{III} or Yb^{III}) show a slight increase in cell death, which indicates some dark toxicity. For the Gd^{III} complex, 7.6% of cells were apoptotic (4.0% early stage and 3.6% late stage), and 5.8% of cells were necrotic, for a total of 13.4% of cell population death in the dark. Similarly, for the Yb^{III} complex, 5.8% of cells were apoptotic (3.1% early stage and 2.7% late stage), and 4.6% of cells were necrotic, which shows a total of 10.4% of cell population death in the dark. These total cell death percentages are similar to those obtained through the MTT assay for dark toxicity (25 μM) (Figure 4).

In contrast, after irradiating the cells incubated with ***2*Thept(COO)$_4^{4-}$** or [Ln***2*Thept(COO)$_4$**]$^-$, both necrotic and apoptotic cell death pathways are observed. For ***2*Thept-(COO)$_4^{4-}$** 16.3% of cells were apoptotic (10.1% early stage and 6.2% late stage), and 7.6% of cells were necrotic. Combined, these values indicate that 24% of the cell population undergoes light-activated cell death.

For the Gd^{III} complex, 55% of the cell population shows light-induced cell death (4.0% early stage apoptosis, 19.4% late stage apoptosis, and 31.6% necrosis). Similarly, for the Yb^{III} complex, 49% of the cell population shows light-induced cell death (2.2% early stage apoptosis, 20.5% late stage apoptosis, and 26.2% necrosis). In analogy to the free ligand, these data suggest both apoptotic and necrotic pathways as well, yet twice the population of dead cells is observed. These findings are consistent to the MTT assay results for phototoxicity at 25 μM.

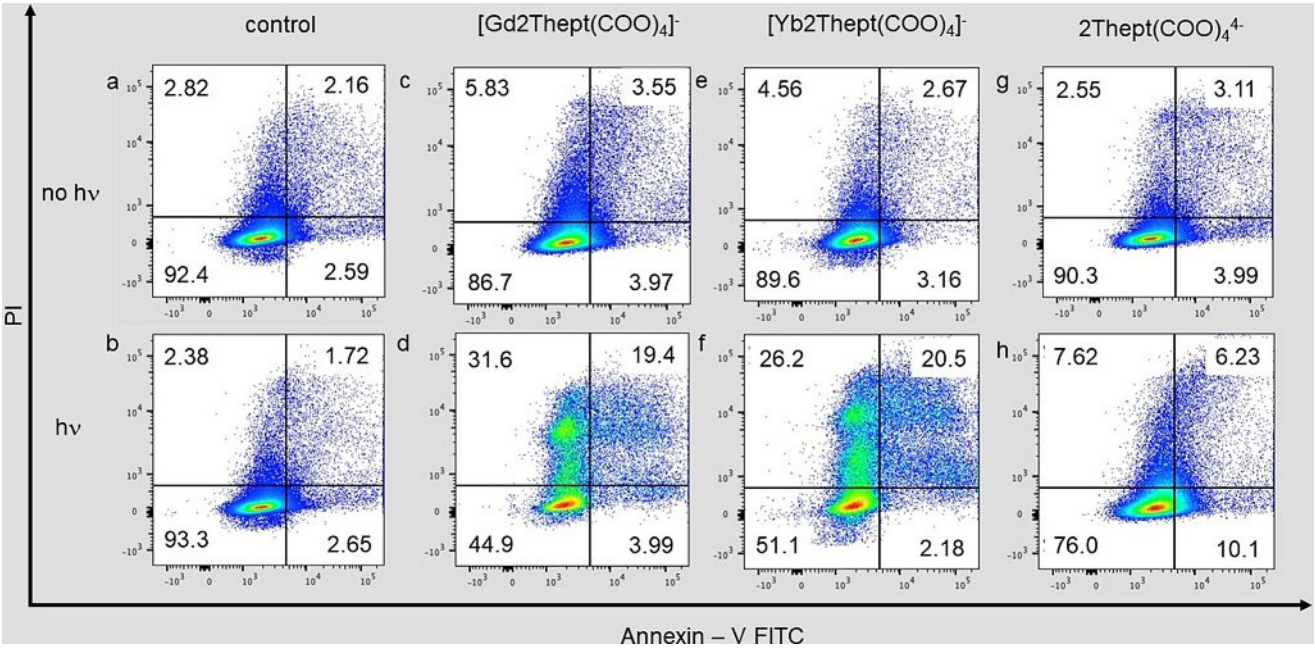

Figure 5. Flow cytometry quantification of Annexin V/PI labelled HeLa cells treated in the dark or with light irradiation (2 minutes of 365 nm): (a) control in the dark; (b) control under light irradiation; (c) [Gd**2Thept(COO)$_4$**]$^-$ (25 μM) in the dark; (d) [Gd**2Thept(COO)$_4$**]$^-$ (25 μM) irradiated with light; (e) [Yb**2Thept-(COO)$_4$**]$^-$ (25 μM) in the dark; (f) [Yb**2Thept(COO)$_4$**]$^-$ (25 μM) irradiated with light; (g) **2Thept(COO)$_4^{4-}$** (25 μM) in the dark; (h) **2Thept(COO)$_4^{4-}$** (25 μM) irradiated with light. PBS buffer was used as a control to accommodate changes in volume during sample preparation.

Conclusions

In this work, we have isolated a series of new complexes containing $^1O_2$-generating oligothiophene moieties. We have shown that these compounds are capable of Ln^{III}-centered emission, and of generating $^1O_2$ with efficiencies comparable to known compounds. We have also explored their phototoxicity and dark toxicity with HeLa cells and determined IC_{50} values under irradiation at 365 nm of 15.2 to 16.2 μM. Further investigation using flow cytometry indicates the presence of both necrotic and late apoptotic cells. In the dark, the compounds are much less cytotoxic towards HeLa cells, with decreases in cell viability to $<10\%$. Although we attribute the cytotoxicity to the formation of $^1O_2$, we cannot rule out the formation of other reactive oxygen species that could contribute as well to the observed cell death.

The dual functionality of these compounds allows for a variety of applications where $^1O_2$ plays a vital role and provides simultaneous tracking of the complexes by Ln^{III}-centered luminescence. While these complexes are water-soluble, attempts to image luminescence within HeLa cells were not fruitful, and is likely due to the low emission efficiencies in aqueous environment. Nonetheless, these compounds provide a design basis for the isolation of compounds with dual functionality, that generate both $^1O_2$ and display the characteristic Ln^{III} emission.

Acknowledgements

The National Science Foundation (CHE 1800392 to AdBD) is gratefully acknowledged for financial support. Shanti Rawat and Carime V. da S. Rodrigues are acknowledged for their support and guidance for biological experiments. Janina S. Ruprecht is acknowledged for her support with mass spectrometry.

Conflict of interest

The authors declare no conflict of interest.

Keywords: dual functionality · lanthanides · luminescence · photodynamic therapy · singlet oxygen

[1] A. T. Hoye, J. E. Davoren, P. Wipf, M. P. Fink, V. E. Kagan, *Acc. Chem. Res.* **2008**, *41*, 87–97.
[2] M. Ethirajan, Y. Chen, P. Joshi, R. K. Pandey, *Chem. Soc. Rev.* **2011**, *40*, 340–362.
[3] a) J. A. Leman, C. A. Morton, *Expert Opin. Biol. Ther.* **2002**, *2*, 45–53; b) *Ophthalmology* **2000**, *107*, 2314–2317.
[4] a) F. Heinemann, J. Karges, G. Gasser, *Acc. Chem. Res.* **2017**, *50*, 2727–2736; b) S. Monro, K. L. Colón, H. Yin, J. Roque, P. Konda, S. Gujar, R. P. Thummel, L. Lilge, C. G. Cameron, S. A. McFarland, *Chem. Rev.* **2019**, *119*, 797–828; c) T. Reynolds, *J. Natl. Cancer Inst.* **1997**, *89*, 112–114.
[5] a) X.-J. Jiang, P.-C. Lo, Y.-M. Tsang, S.-L. Yeung, W.-P. Fong, D. K. P. Ng, *Chem. Eur. J.* **2010**, *16*, 4777–4783; b) P.-C. Lo, J.-D. Huang, D. Y. Y. Cheng, E. Y. M. Chan, W.-P. Fong, W.-H. Ko, D. K. P. Ng, *Chem. Eur. J.* **2004**, *10*, 4831–4838.
[6] F. Dumoulin, M. Durmuş, V. Ahsen, T. Nyokong, *Coord. Chem. Rev.* **2010**, *254*, 2792–2847.

[7] a) H. Dummin, T. Cernay, H. W. Zimmermann, *J. Photochem. Photobio. B* **1997**, *37*, 219 – 229; b) A. E. O'Connor, W. M. Gallagher, A. T. Byrne, *Photochem. Photobiol.* **2009**, *85*, 1053 – 1074.
[8] R. W. Redmond, J. N. Gamlin, *Photochem. Photobiol.* **1999**, *70*, 391 – 475.
[9] R. Baskaran, J. Lee, S.-G. Yang, *Biomater. Res.* **2018**, *22*, 25.
[10] A. de Bettencourt-Dias, *Introduction to Lanthanide Ion Luminescence* (Ed. A. de Bettencourt-Dias), Wiley, Chichester, **2014**, pp. 1 – 48.
[11] S. Dasari, S. Singh, P. Kumar, S. Sivakumar, A. K. Patra, *Euro. J. Med. Chem.* **2019**, *163*, 546 – 559.
[12] J. Jia, Y. Zhang, M. Zheng, C. Shan, H. Yan, W. Wu, X. Gao, B. Cheng, W. Liu, Y. Tang, *Inorg. Chem.* **2018**, *57*, 300 – 310.
[13] F. Xu, Y. Zhao, M. Hu, P. Zhang, N. Kong, R. Liu, C. Liu, S. K. Choi, *Chem. Commun.* **2018**, *54*, 9525 – 9528.
[14] S. Dasari, S. Singh, S. Sivakumar, A. K. Patra, *Chem. Eur. J.* **2016**, *22*, 17387 – 17396.
[15] G.-L. Law, R. Pal, L. O. Palsson, D. Parker, K.-L. Wong, *Chem. Commun.* **2009**, 7321 – 7323.
[16] P. Ung, M. Clerc, H. Huang, K. Qiu, H. Chao, M. Seitz, B. Boyd, B. Graham, G. Gasser, *Inorg. Chem.* **2017**, *56*, 7960 – 7974.
[17] T. Zhang, C.-F. Chan, J. Hao, G.-L. Law, W.-K. Wong, K.-L. Wong, *RSC Adv.* **2013**, *3*, 382 – 385.
[18] K. R. Johnson, A. de Bettencourt-Dias, *Inorg. Chem.* **2019**, *58*, 13471 – 13480.
[19] a) M. Ciofalo, G. Ponterini, *J. Photochem. Photobiol. A: Chemistry* **1994**, *83*, 1 – 6; b) R. Boch, B. Mehta, T. Connolly, T. Durst, J. T. Arnason, R. W. Redmond, J. C. Scaiano, *J. Photochem. Photobiol. A: Chemistry* **1996**, *93*, 39 – 47; c) T. Eicher, S. Hauptmann, A. Speicher, *The Chemistry of Heterocycles: Structures, Reactions, Synthesis and Applications*, Wiley-VCH, Weinheim, **2012**, p. 646 pp; d) R. J. Marles, J. B. Hudson, E. A. Graham, C. Soucy-Breau, P. Morand, R. L. Compadre, C. M. Compadre, G. H. N. Towers, J. T. Arnason, *Photochem. Photobiol.* **1992**, *56*, 479 – 487; e) J. C. Scaiano, A. MacEachern, J. T. Arnason, P. Morand, D. Weir, *Photochem. Photobiol.* **1987**, *46*, 193 – 199; f) J. Pina, J. S. Seixas de Melo, *Phys. Chem. Chem. Phys.* **2009**, *11*, 8706 – 8713; g) F. J. Gommers, J. Bakker, *Bioact. Mol.* **1988**, *7*, 61 – 69; h) A. Parthasarathy, S. Goswami, T. S. Corbitt, E. Ji, D. Dascier, D. G. Whitten, K. S. Schanze, *ACS Appl. Mater. Interfaces* **2013**, *5*, 4516 – 4520; i) R. J. Marles, R. L. Compadre, C. M. Compadre, C. Soucy-Breau, R. W. Redmond, F. Duval, B. Mehta, P. Morand, J. C. Scaiano, J. T. Arnason, *Pestic. Biochem. Physiol.* **1991**, *41*, 89 – 100; j) J. B. Hudson, E. A. Graham, N. Miki, G. H. N. Towers, L. L. Hudson, R. Rossi, A. Carpita, D. Neri, *Chemosphere* **1989**, *19*, 1329 – 1343; k) M. Hekrnreiter, J. Kagan, X. Chen, K. Y. Lau, M. D'Auria, A. Vantaggi, *Photochem. Photobiol.* **1993**, *58*, 49 – 52; l) H. D. Burrows, J. Seixas de Melo, C. Serpa, L. G. Arnaut, A. P. Monkman, I. Hamblett, S. Navaratnam, *J. Chem. Phys.* **2001**, *115*, 9601 – 9606.
[20] L. Lilge, M. Roufaiel, S. Lazic, P. Kaspler, M. A. Munegowda, M. Nitz, J. Bassan, A. Mandel, *Translational Biophotonics* **2020**, e201900032.
[21] A. L. Capodilupo, V. Vergaro, F. Baldassarre, A. Cardone, G. A. Corrente, C. Carlucci, S. Leporatti, P. Papadia, G. Gigli, G. Ciccarella, *Biochim. Biophys. Acta Gen. Subj.* **2015**, *1850*, 385 – 392.
[22] a) K. R. Johnson, S. B. Vittardi, M. A. Gracia-Nava, J. J. Rack, A. de Bettencourt-Dias, *Chem. Eur. J.* **2020**, *26*, 7274 – 7280; b) K. R. Johnson, S. B. Vittardi, M. A. Gracia-Nava, J. Rack, A. de Bettencourt Dias, *unpublished results* **2020**.
[23] a) K. Liu, X. Yan, Y.-J. Xu, L. Dong, L.-N. Hao, Y.-H. Song, F. Li, Y. Su, Y.-D. Wu, H.-S. Qian, W. Tao, X.-Z. Yang, W. Zhou, Y. Lu, *Biomater. Sci.* **2017**, *5*, 2403 – 2415; b) T. Vairapperumal, A. Saraswathy, J. S. Ramapurath, S. Kalarical Janardhanan, N. Balachandran Unni, *Sci. Rep.* **2016**, *6*, 34976.
[24] L. Pellegatti, J. Zhang, B. Drahos, S. Villette, F. Suzenet, G. Guillaumet, S. Petoud, É. Tóth, *Chem. Commun.* **2008**, 6591 – 6593.
[25] a) S. Laine, C. S. Bonnet, F. K. Kálmán, Z. Garda, A. Pallier, F. Caillé, F. Suzenet, G. Tircsó, É. Tóth, *New J. Chem.* **2018**, *42*, 8012 – 8020; b) C. S. Bonnet, F. Buron, F. Caillé, C. M. Shade, B. Drahoš, L. Pellegatti, J. Zhang, S. Villette, L. Helm, C. Pichon, F. Suzenet, S. Petoud, É. Tóth, *Chem. Eur. J.* **2012**, *18*, 1419 – 1431; c) C. S. Bonnet, S. Laine, F. Buron, G. Tircsó, A. Pallier, L. Helm, F. Suzenet, É. Tóth, *Inorg. Chem.* **2015**, *54*, 5991 – 6003.
[26] a) R. Xiong, A.-B. Bornhof, A. I. Arkhypchuk, A. Orthaber, K. E. Borbas, *Chem. Eur. J.* **2017**, *23*, 4089 – 4095; b) K. L. Woon, A. Ariffin, K. W. Ho, S.-A. Chen, *RSC Adv.* **2018**, *8*, 9850 – 9857.
[27] C.-C. Ko, V. W.-W. Yam, *Acc. Chem. Res.* **2018**, *51*, 149 – 159.
[28] J. H. S. K. Monteiro, D. Machado, L. M. de Hollanda, M. Lancellotti, F. A. Sigoli, A. de Bettencourt-Dias, *Chem. Commun.* **2017**, *53*, 11818 – 11821.
[29] a) J.-C. G. Bünzli, G. R. Choppin, *Lanthanide Probes in Life, Chemical and Earth Sciences: Theory and Practice*, Elsevier, Amsterdam, **1989**; b) J. C. G. Bünzli, *Rare Earth Luminescent Centers in Organic and Biochemical Compounds*, Vol. 83 (Eds.: G. Liu, B. Jacquier), Springer, Berlin, **2005**, pp. 462 – 499.
[30] a) W. D. J. Horrocks, D. R. Sudnick, *Acc. Chem. Res.* **1981**, *14*, 384 – 392; b) W. D. H. R. M. Supkowski, *Inorg. Chim. Acta* **2002**, *340*, 44 – 48.
[31] C. Gunanathan, Y. Diskin-Posner, D. Milstein, *Crys. Growth Des.* **2010**, *10*, 4235 – 4239.
[32] a) Z. Zhang, Y. Zhou, H. Li, T. Gao, P. Yan, *Dalton Trans.* **2019**, *48*, 4026 – 4034; b) Y.-G. Wang, Y.-Q. Li, H.-H. Tang, L.-R. Lin, L.-H. Ma, *ACS Omega* **2018**, *3*, 5480 – 5490.
[33] H. Ramesh, T. Mayr, M. Hobisch, S. Borisov, I. Klimant, U. Krühne, J. M. Woodley, *J. Chem. Technol. Biotechnol.* **2016**, *91*, 832 – 836.
[34] T. Sato, Y. Hamada, M. Sumikawa, S. Araki, H. Yamamoto, *Ind. Eng. Chem. Res.* **2014**, *53*, 19331 – 19337.
[35] a) M. Galland, T. Le Bahers, A. Banyasz, N. Lascoux, A. Duperray, A. Grichine, R. Tripier, Y. Guyot, M. Maynadier, C. Nguyen, M. Gary-Bobo, C. Andraud, C. Monnereau, O. Maury, *Chem. Eur. J.* **2019**, *25*, 9026; b) M. Galland, F. Riobé, J. Ouyang, N. Saleh, F. Pointillart, V. Dorcet, B. Le Guennic, O. Cador, J. Crassous, C. Andraud, C. Monnereau, O. Maury, *Eur. J. Inorg. Chem.* **2019**, 118 – 125.
[36] L. B. Josefsen, R. W. Boyle, *Theranostics* **2012**, *2*, 916 – 966.
[37] a) T. I. Malinin, V. P. Perry, *Cryobiology* **1967**, *4*, 90 – 96; b) M. Timm, L. Saaby, L. Moesby, E. W. Hansen, *Cytotechnology* **2013**, *65*, 887 – 894.
[38] B. P. Lucey, W. A. Nelson-Rees, G. M. Hutchins, *Arch. Pathol. Lab Med.* **2009**, *133*, 1463 – 1467.
[39] J. van Meerloo, G. J. L. Kaspers, J. Cloos in *Cell Sensitivity Assays: The MTT Assay* (Ed.: I. A. Cree), Humana, Totowa, **2011**, pp. 237 – 245.
[40] E. Delaey, F. van Laar, D. De Vos, A. Kamuhabwa, P. Jacobs, P. de Witte, *J. Photochem. Photobiol. B* **2000**, *55*, 27 – 36.

Manuscript received: March 31, 2020
Revised manuscript received: April 22, 2020
Accepted manuscript online: April 23, 2020
Version of record online: August 18, 2020